Multicarrier-CDMA STAR with Time and Frequency Synchronization

Besma Smida, Sofiène Affes, Jun Li, and Paul Mermelstein
INRS-EMT, University of Quebec, Montreal, Canada

***Abstract*— This paper proposes a spectrum-efficient spatio-temporal array-receiver (STAR) for multi-carrier CDMA systems named MC-STAR. First, we derive a new post-correlation model for MC-CDMA that supports both the MT-CDMA and MC-DS-CDMA air-interfaces. Based on this model, we introduce a new multi-carrier receiver with rapid and accurate joint synchronization in time and frequency. We also exploit the intrinsic subcarrier correlation to improve the channel identification and the synchronization operations. We analyze the performance of MC-STAR in an unknown time-varying Rayleigh channel with multipath, carrier offset and cross-correlation between subcarrier channels. Simulation results confirm the accuracy of the joint time/frequency synchronization. They also confirm that for each MC-STAR configuration there exists an optimum number of subcarriers which results in maximum throughput. A higher number of subcarriers increases the inter-carrier interference while a lower number of subcarriers reduces the frequency gain. With four receiving antennas and five MT-CDMA subcarriers in 5 MHz bandwidth, MC-STAR provides about 1.2 bps/Hz at low mobility for DBPSK, i.e., an increase of 30% in spectrum efficiency over DS-CDMA.**

I. Introduction

One important challenge for future wireless networks is the design of appropriate transceivers that can reliably transmit high data rates at a high bandwidth efficiency. Multi-carrier (MC)-CDMA systems in particular have received considerable attention, because they have the attractive feature of high spectral efficiency and because they can be easily implemented using the fast fourier transform (FFT) without significantly increasing the transmitter and receiver complexities [1].

However promising, challenges remain before MC-CDMA can achieve its full potential. MC-CDMA, similar to other multi-carrier schemes, is sensitive to the signal distortion generated by the imperfect frequency down-conversion at the receiver due to local oscillator frequency offset. It has been found that carrier frequency offset (CFO) gives rise to a reduction of the useful signal power and to the inter-carrier interference (ICI) [2]. In addition to the degradation induced by the CFO, an MC-CDMA signal experiences inter-symbol interference (ISI) caused by the multipath effect. In order to enjoy all the benefits of multi-carrier transmission, two key tasks must be successfully accomplished: 1) multipath channel identification and equalization and 2) carrier frequency offset estimation and recovery (CFOR). Carrier synchronization and channel identification have traditionally been treated as separate problems. Most research on channel identification implicitly assumes that the carrier offset has been properly compensated [3]. Similarly, many existing CFOR techniques consider only flat channels [4], [5], [6]. Some works have investigated the joint estimation of multipath and carrier offset for MC-CDMA systems [7], [8], but to the authors' best knowledge, no such investigations are available for MC-DS-CDMA or MT-CDMA systems.

We propose a new MC-CDMA receiver [9] that supports both MC-DS-CDMA and multitone (MT)-CDMA. It performs blind channel identification and equalization as well as fast and accurate joint synchronization in time and frequency using a simple linear regression (LR) technique. We extend the post-correlation model (PCM) in [10] to MC-CDMA air-interface by characterizing the structure of the channel in space, time, and frequency [9]. Based on this model, named multi-carrier PCM (MC-PCM), we propose a new multi-carrier spatio-temporal array-receiver (MC-STAR). Single-carrier STAR has previously shown a significant performance advantage over Rake-type receivers both in channel identification and synchronization [10]. We therefore exploit its basic structure to implement spatio-temporal channel identification, the acquisition and the tracking of the multipaths on each subcarrier. However, we introduce a joint time-delay and frequency synchronization module because of the sensitivity of MC-CDMA to the CFO. In addition, we exploit the subcarrier correlation, intrinsic to a multi-carrier system, to implement joint multi-carrier channel identification and synchronization operations with significantly improved performance. The common parameters can be estimated more accurately by averaging their estimates over all subcarriers. These parameters include the number of multipaths, their corresponding time-delays and the frequency offset. Other channel parameters, such as the fading coefficients, are correlated but not identical over all subcarriers. Therefore, combining them may not achieve the expected performance enhancement. We thus introduce a moving average technique over strongly-correlated subcarriers. All the parameter estimates are equally weighted and combined through summation. Since estimation errors can be assumed uncorrelated across subcarriers, joint estimation by averaging provides a type of *frequency gain* in a joint multi-carrier estimation process.

Both the design and the assessment of the new MC-STAR are oriented towards real-world implementation. Unlike most evaluations of MC-DS-CDMA or MT-CDMA systems which assume independent or identical characteristic fading at each received subcarrier [11],[12],[13], we assume correlated Rayleigh channels across subcarriers. Additionally, we analyze the performance of MC-STAR using very realistic link-level simulation setups that take into account time and

0-7803-8938-7/05/$20.00 (C) 2005 IEEE

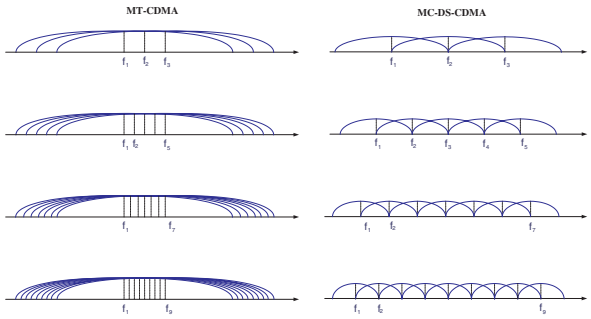

Fig. 1. Different configurations of MT-CDMA and MC-DS-CDMA within the same bandwidth.

frequency mismatch, imperfect power control, channel identification errors etc. Simulation results confirm the accuracy of the joint time/frequency synchronization. The gains in spectrum efficiencies attainable by MC-STAR are significant and are evaluated in the paper as a function of the number of subcarriers and modulation.

II. System Model and Assumptions

A. MC-CDMA Transmitter

The input information sequence is first converted into $N_c = 2K + 1$ parallel[1] data sequences $b_{-K,n}, \ldots, b_{0,n}, \ldots, b_{K,n}$ where n is the time index. The data $b_{k,n} \in C_{\mathcal{M}}$ (i.e., constellation set) is $\mathcal{M}$-PSK modulated and differentially[2] encoded at rate $1/T_{MC}$, where $T_{MC} = N_c \times T$ is the symbol duration after serial/parallel (S/P) conversion. The resulting S/P converter output is then spread with a long spreading code $c(t)$ at a rate $1/T_c$. The spreading factor, defined as the ratio between the chip rate and the symbol rate is $L = \frac{T_{MC}}{T_c}$. Closed-loop power control is taken into account at the transmitter by the amplification factor $a_k(t)$. All the data are then modulated in baseband by the inverse discrete Fourier transform (IDFT) and added to obtain the multi-carrier signal. A guard interval T_g is then inserted between symbols to avoid intersymbol interference caused by multipath fading. The new symbol duration is hence $T_G = T_{MC} + T_g = (L + L_g) \times T_c$. Finally the signal is transmitted after pulse shaping and radio-frequency up-conversion.

The modulated subcarriers are orthogonal over the symbol duration T_{MC}. The frequency corresponding to the k-th subcarrier is $f_k = \lambda \times k/T_{MC}$. The transmitter belongs to the family of MT-CDMA if λ is set to 1, and to the class of MC-DS-CDMA if λ is set to L (see resulting spectra in Fig. 1).

B. Channel Model

We consider transmission to M receiving antennas[3]. The channel is assumed to be a slowly varying frequency selective Rayleigh channel with delay spread $\Delta\tau$. We note here that the large-scale path-loss that includes free-space path-loss and shadowing is the same for all subcarriers. Moreover the number of resolvable paths P and their propagation time-delays $\tau_1, \ldots, \tau_P$ depend on the reflecting objects and scatterers and therefore can be assumed equal for all subcarriers [15]. We assume correlated Rayleigh channels across subcarriers and adopt the approach proposed in [16] to generate it. We also assume that the received channel multipath components across the M antennas are independent.

C. Extension of the Post-Correlation Model to MC-CDMA

We provide in this section an extension of the post correlation model derived for DS-CDMA systems in [10], to the multi-carrier case. To retrieve $b_{k,n}$ for the k-th subcarrier at the receiver, we decorrelate the received signal with the spreading sequence and sample it at the chip rate over the interval[4] $t \in [T_g,\ T)$ to form the $M \times L$ post-correlated observation matrix:

$$\begin{aligned} \mathbf{Z}_{k,n} &= s_{k,n}\mathbf{H}_{k,n} + \mathbf{N}_{k,n} \\ &= s_{k,n}e^{j2\pi\Delta f n T_G}\mathbf{G}_{k,n}\boldsymbol{\Upsilon}_{k,n}\mathbf{D}_{k,n}^T + \mathbf{N}_{k,n}, \end{aligned} \tag{1}$$

where $s_{k,n} = b_{k,n}\psi_{k,n}$ is the signal component on the k-th subcarrier and $\psi_{k,n}^2$ is the total power received over the k-th subcarrier. Δf models the CFO, which is assumed equal for all subcarriers. This is a realistic assumption since there is only one oscillator per receiver. $\mathbf{H}_{k,n}$ is $M \times L$ spatio-temporal propagation channel matrix normalized to $\sqrt{M}$. $\mathbf{J}_{k,n} = e^{j2\pi\Delta f n T_G}\mathbf{G}_{k,n}\boldsymbol{\Upsilon}_{k,n}$ is the spatial response matrix. It corresponds to the propagation matrix $\mathbf{G}_{k,n}$ multiplied by the diagonal matrix of power partition over multipaths $\boldsymbol{\Upsilon}_{k,n} = \text{diag}\{\epsilon_{k,1,n}, \ldots \epsilon_{k,p,n}, \ldots \epsilon_{k,P,n}\}$ and affected by a common carrier phase error due to the frequency offset. $\mathbf{N}_{k,n}$ is the additive noise plus interference matrix. $\mathbf{D}_{k,n} = [D_{k,1}, ..., D_{k,P}]$ is the time response matrix, where $D_{k,p} = e^{-j2\pi k\tau_p/T}[\rho_c(-\tau_p), \rho_c(T_c - \tau_p)e^{j2\pi k/L}, \ldots, \rho_c((L-1)T_c - \tau_p)e^{j2\pi k(L-1)/L}]^T$ is the time-delay impulse response of path p sampled at $1/T_c$ on the k-th subcarrier. $\rho_c(t)$ is the correlation function of the chip pulse. The matrices $\mathbf{Z}_{k,n}$, $\mathbf{H}_{k,n}$ and $\mathbf{N}_{k,n}$ are transformed into (ML)-dimensional vectors by concatenating their columns, yielding $\underline{Z}_{k,n} = \underline{H}_{k,n}s_{k,n} + \underline{N}_{k,n}$, where $\underline{Z}_{k,n}$, $\underline{H}_{k,n}$ and $\underline{N}_{k,n}$ denote the resulting vectors. This equation provides a new data block model for MC-CDMA systems similar to the PCM derived for DS-CDMA. The key difference of the new MC-PCM is the reformulation of the time-response matrix $\mathbf{D}_{k,n}$ and the spatial-response matrix $\mathbf{J}_{k,n}$ [17]. Based on this model, we will introduce in the next section the new MC-STAR with joint time-delay and frequency synchronization.

III. Proposed Multicarrier CDMA Spatio-Temporal Array-Receiver: MC-STAR

A. Spatio-Temporal Channel Identification and Combining

At each iteration n, we assume for each subcarrier with index k that we have an estimate $\underline{\tilde{H}}_{k,n}$ of the spatio-temporal

[1] We selected an odd number to have a central frequency, but the model can easily be rearranged to operate with an even number.

[2] We can also use pilot symbols for coherent modulation and detection [14], but that is beyond the scope of this paper.

[3] It could be applied to both uplink and downlink transmission.

[4] We dropped $Z_{k,l}(t)$ over the time interval $t \in [0,\ T_g)$ at the receiver.

propagation channel $\underline{H}_{k,n}$. From this estimate, we extract the signal component $s_{k,n}$ by spatio-temporal MRC:

$$\tilde{s}_{k,n} = \frac{\tilde{\underline{H}}^H_{k,n}\underline{Z}_{k,n}}{M}. \quad (2)$$

Hence, we estimate the total power received from the desired user on the k-th subcarrier for power control (PC) by $\hat{\psi}^2_{k,n} = (1-\alpha)\hat{\psi}^2_{k,n-1} + \alpha|\tilde{s}_{k,n}|^2$, where $\alpha \ll 1$ is a smoothing factor for power estimation. Since in the case of a multi-carrier system each subcarrier is subject to different channel fading, two alternative power-control techniques can be considered. The first is per-carrier PC where we transmit more power on the subcarrier which suffers from deep fading and less power on the subcarrier which suffers from less fading. The second one is all-carrier PC where we calculate the total received power over all subcarriers and accordingly jointly decrease or increase the transmission power for all subcarriers. In [9], we have shown that the per-carrier power control scheme performs better than the all-carrier one for both MC-DS-CDMA and MT-CDMA. Hence, in what follows, we consider only the per-carrier PC technique.

After power estimation, we reconstruct the differentially encoded signal estimate $\hat{s}_{k,n}$ of the signal component $s_{k,n}$ after hard decision over $\tilde{s}_{k,n}$ as:

$$\hat{s}_{k,n} = \hat{\psi}_{k,n} \arg \min_{c_m \in C_{\mathcal{M}}} \|\tilde{s}_{k,n} - c_m\|^2, \quad (3)$$

then feed it back in a decision feedback identification (DFI) scheme to update the channel estimate as follows:

$$\tilde{\underline{H}}_{k,n+1} = \tilde{\underline{H}}_{k,n} + \mu(\underline{Z}_{k,n} - \tilde{\underline{H}}_{k,n}\hat{s}_{k,n})\hat{s}^*_{k,n}, \quad (4)$$

where μ is an adaptation step-size. This DFI blind identification procedure estimates the channel within a constellation-invariant phase ambiguity [14]. Since b_n is differentially encoded, this ambiguity has no consequences.

B. Time-Delay and Frequency Acquisition

The joint operation of time-delay and frequency synchronization is implemented in two steps. First, we estimate the number of multipaths $\hat{P}$, their time delays, and their magnitude. Then, we determine the carrier-frequency offset. Based on this information, an estimate of the spatio-temporal channel is made, and the process is iterated. Key to the algorithm presented is the space/time separation of the channel that enables us to decouple time and carrier-frequency synchronization. The variation of multipath time-delays affects only the matrix $\mathbf{D}_{k,n}$ and the carrier-frequency offset intervenes only in the phase of each (m,p)-coefficient of $\mathbf{J}_{k,n}$. Based on this observation, we propose the following algorithm for joint time and frequency synchronization over each subcarrier.

1) Initial multipath detection: In the acquisition mode, the channel identification procedure converges to a rough estimate of the spatio-temporal channel $\tilde{\mathbf{H}}_{k,n}$ as in [18]. From this estimate, we define a localization spectrum over the possible multipath delays. Then we detect the number of multipaths $\hat{P}_k$ and estimate their time-delays $\hat{\tau}_{k,p}$ from the strongest peaks of the spectrum. We assumed earlier that the propagation time-delays are the same for all subcarriers. Therefore, we can exploit the frequency gain (cf. section IV-C) to minimize the estimation errors by averaging the localization spectrum as follows[5]:

$$S(lT_c) = \sum_{k=-K}^{K} S_k(lT_c)/N_c = \sum_{k=-K}^{K} \|\tilde{H}_{n,k,l}\|^2/N_c. \quad (5)$$

Once the number of multipath $\hat{P}$ and their time-delays $\hat{\tau}_{p,n}$ are estimated from $S(lT_c)$, we build the time-response matrix $\hat{\mathbf{D}}^T_{k,n}$ using its matrix structure detailed below Eq. (1).

2) Separation of the spatial response matrix $\hat{\mathbf{J}}_{k,n}$: From $\hat{\mathbf{D}}^T_{k,n}$ we next estimate $\tilde{\mathbf{J}}^T_{k,n} = (\hat{\mathbf{D}}^T_{k,n}\hat{\mathbf{D}}_{k,n})^{-1}\hat{\mathbf{D}}^T_{k,n}\tilde{\mathbf{H}}^T_{k,n}$ [10]. If the fading among the subcarriers is highly correlated, we can once again exploit the frequency gain (cf. section IV-C) and introduce a moving average technique over subcarriers to provide an enhanced estimate:

$$\hat{\mathbf{J}}_{k,n} = \frac{1}{2K_f+1}\sum_{k'=-K_f}^{K_f} \tilde{\mathbf{J}}_{k+k',n}, \quad (6)$$

where the averaging window span K_f determines the number of highly-correlated subcarriers to be considered in the moving average. The matrix $\hat{\mathbf{J}}_{k,n}$ is then transformed into an (MP)-dimensional vector $\underline{\hat{J}}_{k,n}$ by concatenating its columns. We represent the i-th element $\underline{\hat{J}}_{i,k,n} = \hat{r}_{i,k,n}e^{j\hat{\phi}_{i,k,n}}$ by its magnitude $\hat{r}_{i,k,n}$ and its phase $\hat{\phi}_{i,k,n}$.

3) Carrier frequency acquisition: We earlier assumed that the channel parameters remain unchanged over periods of, say, R symbols while a fixed phase shift (due to carrier offset) is introduced between two samples. We hence buffer the phases of each i-coefficient of $\underline{\hat{J}}_{k,n}$ over R symbols and apply a LR-based procedure to estimate Δf [9]. For each diversity finger for $i = 1,\ldots,MP$, we form the vector $\hat{\Phi}_{i,k,nR} = [\hat{\phi}_{i,k,(n-1)R+1},\ldots,\hat{\phi}_{i,k,nR}]$, then estimate Δf at the symbol iteration nR as the slope of a linear regression as follows:

$$\widehat{\Delta f}_{i,k,nR} = \frac{\|R_0\|^2(R_1^T\hat{\Phi}_{i,k,nR}) - (R_1^TR_0)(R_0^T\hat{\Phi}_{i,k,nR})}{2\pi T\{\|R_0\|^2\|R_1\|^2 - (R_1^TR_0)^2\}}, \quad (7)$$

where $R_0 = [1,\ldots,1]$ and $R_1 = [1,\ldots,r,\ldots,R]$. Thus, there are MP estimates of the frequency offset for each subcarrier. We exploit space-time-frequency diversity and minimize estimation errors, by a weighted summation over these $M\times P\times N_c$ estimates[6]:

$$\widehat{\Delta f}_{nR} = \frac{\sum_{k=-K}^{K}\sum_{i=1}^{MP}\bar{r}^2_{i,k,(n-1)R+r}\widehat{\Delta f}_{i,k,nR}}{N_c\sum_{i=1}^{MP}\bar{r}^2_{i,k,(n-1)R+r}}. \quad (8)$$

This step allows the estimation of the frequency offset while exploiting diversity over three dimensions: time, space and frequency. This idea, which is to our knowledge first explored in the framework of this contribution [9], significantly improves the performance of MC-STAR (cf. section IV-C).

[5]We can still apply the same procedure if P_k and τ_k were assumed different over subcarriers by exploiting $S_k(pT_c)$ and disabling averaging over subcarriers.

[6]We can still apply the same procedure if Δf were different over antennas or subcarriers by restricting averaging in Eq. (8) over the appropriate dimensions.

4) Reconstruction of the spatio-temporal channel: We reconstruct the spatio-temporal propagation matrix $\hat{\mathbf{H}}_{k,n}$ by $\hat{\mathbf{H}}_{k,n} = \hat{\mathbf{J}}_{k,n}\hat{\mathbf{D}}^T_{k,n}$. $\hat{\mathbf{H}}_{k,n}$ replaces the coarse estimate $\tilde{\mathbf{H}}_{k,n}$ and it is considered as an initial estimate for the tracking module. Once an estimate of the carrier frequency offset estimate $\widehat{\Delta f}$ is available at iteration $R+1$, we implement carrier frequency offset recovery (CFOR) in a closed-loop structure, where we feed back the estimate of the frequency offset to the input of MC-STAR:

$$\dot{\underline{Z}}_{k,n} = e^{-j2\pi\Delta f n T_G}\underline{Z}_{k,n} = \dot{\underline{H}}_{k,n}s_{k,n} + \dot{\underline{N}}_{k,n}, \qquad (9)$$

where $\dot{\underline{H}}_{k,n}$ is the channel vector including CFOR (i.e., $\dot{\mathbf{H}}_{k,n} = \dot{\mathbf{J}}_{k,n}\mathbf{D}^T_{k,n}$) and $\dot{\underline{N}}_{k,n}$ is the interference vector within a constant phase rotation. The CFOR in Eq. (9) reduces the time-variations in $\underline{H}_{k,n}$ due to Δf to much weaker fluctuations in $\dot{\underline{H}}_{k,n}$ due to the residual $\delta f_{nR} = \Delta f_{nR} - \widehat{\Delta f}_{nR}$. Tracking of $\dot{\underline{H}}_{k,n}$ instead of $\underline{H}_{k,n}$ results in much weaker identification errors and enables further reduction of the carrier frequency estimation error δf.

C. Time-Delay and Frequency-Offset Tracking

The channel considered is time-varying. Therefore, in order to keep channel identification accurate after acquisition, we need to update the space/time separation and reconstruction of the channel to the time-variations of time-delays and frequency offset. Hence, we modify the channel identification of Eq. (4) to take into account the frequency offset compensation in Eq. (9) as follows, for $n > R+1$:

$$\tilde{\dot{\underline{H}}}_{k,n+1} = \hat{\dot{\underline{H}}}_{k,n} + \mu(\dot{\underline{Z}}_{k,n} - \hat{\dot{\underline{H}}}_{k,n}\hat{s}_{k,n})\hat{s}^*_{k,n}, \qquad (10)$$

where $\hat{s}_{k,n}$ is estimated by hard decision over $\tilde{s}_{k,n} = \hat{\dot{\underline{H}}}^H_{k,n}\dot{\underline{Z}}_{k,n}/M$.

The tracking module of MC-STAR repeatedly updates the number of multipaths, their time-delays and the carrier frequency offset. It allows the reconstruction of an enhanced estimate $\hat{\dot{\underline{H}}}_{k,n+1}$ from $\tilde{\dot{\underline{H}}}_{k,n+1}$ and it is implemented by the following joint time-delay and frequency tracking loop.

1) Tracking the number of multipaths: In order to update the identified number of multipaths, we drop or add a multipath by comparing its energy to specified thresholds [18]. For detecting a vanishing path, we only need to check if for a number of previous block iterations, the received signal power $\sum_{k=-K}^{K}\psi^2_{k,n}\epsilon^2_{k,p,n}$ continuously remains below the threshold. Note that the threshold is defined as a function of the residual noise estimate on all subcarriers. For detecting an appearing path, we check the path energy over the chip-sampled residual spectrum in [18] averaged here (cf. section IV-C) over all subcarriers.

2) Tracking the multipath delays: We update the time response matrix $\hat{\mathbf{D}}_{k,n}$ with subspace-tracking [10]:

$$\tilde{\mathbf{D}}_{k,n+1} = \hat{\mathbf{D}}_{k,n} + \frac{\eta}{M}(\hat{\dot{\mathbf{H}}}^T_{k,n} - \hat{\mathbf{D}}_{k,n}\hat{\dot{\mathbf{J}}}^T_{k,n})\hat{\dot{\mathbf{J}}}^*_{k,n+1}, \qquad (11)$$

where $\hat{\dot{\mathbf{J}}}_{k,n+1}$ is the moving average in Eq. (6) of $\tilde{\dot{\mathbf{J}}}^T_{k,n+1}$. Unlike [10], we can not implement time-delay tracking by linear regression directly over the phase of the column-wise FFT of $\hat{\mathbf{D}}_{k,n}$ and $\tilde{\mathbf{D}}_{k,n+1}$. Hence, we define $\tilde{\boldsymbol{\mathcal{D}}}^c_{k,n+1}$ as the column-wise FFT of $\tilde{\mathbf{D}}^c_{k,n+1}$, with p-th column $\tilde{D}^c_{k,p,n+1} = \tilde{D}_{k,p,n+1} \odot [1, e^{-j2\pi k(1/L)}, \ldots, e^{-j2\pi k((L-1)/L)}]^T$, and $\hat{\boldsymbol{\mathcal{D}}}^c_{k,n}$ as the column-wise FFT of $\hat{\mathbf{D}}^c_{k,n}$, with p-th column $\hat{D}^c_{k,p,n} = \hat{D}_{k,p,n} \odot [1, e^{-j2\pi k(1/L)}, \ldots, e^{-j2\pi k((L-1)/L)}]^T$. By introducing this intermediate transformation of the time responses, we can now estimate the multi-path delays $\hat{\tau}_{k,p,n+1}$ for $k = -K, \ldots, K$ and $p = 1, \ldots, \hat{P}$ by linear regressions of the phase variations between the L components of $\tilde{\mathcal{D}}^c_{k,p,n+1}$ and $\hat{\mathcal{D}}^c_{k,p,n}$ as in [10]. We assumed earlier that the propagation time-delays are the same for all subcarriers. Therefore, we can exploit the frequency gain to minimize the estimation errors by averaging time-delays over carriers as follows:

$$\hat{\tau}_{p,n+1} = \sum_{k=-K}^{K}\hat{\tau}_{k,p,n+1}/N_c, \qquad (12)$$

and hence we rebuild the time-response matrix $\hat{\mathbf{D}}^T_{k,n+1}$ more accurately. This step allows the reconstruction of the spatio-temporal propagation vector $\hat{\mathbf{H}}_{k,n+1} = \hat{\mathbf{J}}_{k,n+1}\hat{\mathbf{D}}^T_{k,n+1}$ with significantly reduced channel identification errors (cf. section IV-C).

3) Tracking the frequency offset: Similarly to frequency offset acquisition, we estimate the carrier frequency offset error $\widehat{\delta f}_{nR}$ by linear regression over successive blocks of length R by replacing $\widehat{\Delta f}_{i,k,nR}$ and $\widehat{\Delta f}_{nR}$ by $\widehat{\delta f}_{i,k,nR}$ and $\widehat{\delta f}_{nR}$ in Eqs. (7) and (8), respectively, and $\Phi_{i,k,nR}$ by $\dot{\Phi}_{i,k,nR}$ in both equations, where $\dot{\Phi}_{i,k,nR}$ is the phase of the i-th coefficient $\hat{\underline{J}}_{i,k,n} = \hat{r}_{i,k,n}e^{j\hat{\phi}_{i,k,n}}$ of the spatial-vector $\hat{\underline{J}}_{k,n}$. The latter is derived from the spatial response matrix $\dot{\mathbf{J}}_{k,n}$ of the carrier-offset-compensated channel $\dot{\mathbf{H}}_{k,n}$. Finally, we update the frequency-offset estimate in Eq. (9) as $\widehat{\Delta f}_{nR+1} = \widehat{\Delta f}_{nR} + \widehat{\delta f}_{nR}$.

IV. Performance Analysis

A. Simulation Setup

In order to compare the performance of MT-CDMA, MC-DS-CDMA, and DS-CDMA, the fading channel parameters, the system data rate, the bandwidth, the link-level curves and the throughput must be taken into consideration. For this reason we fixed the parameters so that all three systems have the same channel parameters and almost the same bandwidth. The simulation parameters common to all multi-carrier system configurations are listed in Table I. We select $\Delta f = 200$ Hz because it is the maximum error tolerated by 3G standards. In [9], we have shown that the length of the guard interval does not affect the link-level performance due to the multipath equalization capability of MC-STAR. We hence fixed $L_g = 0$ in Table I. Table II shows the parameters specific to each multi-carrier CDMA configuration. We choose as a reference the DS-CDMA ($N_c = 1$) system with spreading factor $L = 64$ and chip rate of 3.84 Mcps. We assume frequency selective fading with $P = 3$ propagation paths. One of the features of MT-CDMA is that for constant bandwidth the ratio between the spreading factor L and $2K = N_c - 1$ is constant. We hence maintain the same chip rate (3.840 Mcps) by changing the spreading factor and the number of subcarriers as shown in Fig. 1. We consider four MT-CDMA configurations. Since

Parameter	Value	Comment
BW_{max}	5 MHz	maximum bandwidth
M	4	number of antennas
f_c	1.9 GHz	central carrier frequency
f_D	8.8/88 Hz	Doppler frequency (5 kmph)
Δf	200 Hz	frequency offset
f_{PC}	1600 Hz	frequency of PC updating
Δ_{PC}	± 0.25 dB	power control adjustment
PC_{min}^{max}	± 30 dB	power control range
BER_{PC}	5%	simulated PC bit error rate
$\frac{\delta\tau}{\delta t}$	0.049 ppm	time-delay drift
$\Delta\tau$	4 chips	delay spread
R	64	regression length
β	0	roll-off factor
L_g	0	guard interval length

TABLE I

SIMULATION PARAMETERS.

they use the same chip rate, there are three paths in each MT-CDMA subcarrier. For a fair comparison among different configurations of MC-DS-CDMA, the bandwidth should be the same. By reducing the chip rate, we varied the number of subcarriers while maintaining the orthogonality between them, as illustrated in Fig. 1. Due to the reduction in bandwidth, each subcarrier in MC-DS-CDMA has either two paths or one path (i.e., frequency nonselective fading) for $N_c = 3$ and $N_c \geq 5$, respectively. The main performance criterion is the SNR required per carrier to meet a BER of 5% in order to achieve a QoS of 10^{-6} after channel decoding. The user's data rate is calculated by adding the data rates over all subcarriers.

B. Performance Evaluation of Joint Time-Delay and Frequency-Offset Synchronization

We consider DBPSK MC-STAR modulated data with three subcarriers and a spreading factor of 128 ($N_c = 3$, $L = 128$). The system operates at $SNR_{in} = -3$ dB after despreading. The performance of the joint time-delay and frequency-offset synchronization is plotted in Fig. 2. Fig. 2-a illustrates the time-delay tracking performance (the delays in T_c are initially set to (8, 10, 12)). It clearly shows the stability and the accuracy achieved during the tracking of the three equal-power paths within a standard deviation error of 0.05 chips. In Fig. 2-b we illustrate acquisition and tracking of the frequency offset. The solid line indicates the exact value of the frequency offset. The semi-dashed curve shows that the estimated frequency offset converges relatively fast, after about 256 symbols, to the desired value within a standard deviation error of 5×10^{-4} (i.e., about 15 Hz).

C. Impact of Frequency Gain on Channel Identification Error

In Fig. 3, we plot the average over time and over subcarriers of the channel identification error of MC-STAR with joint multi-carrier channel identification and synchronization (i.e., with frequency gain) for $N_c = 5$ (see Table III). We also plot the average identification error that would result from hypothetical application of N_c independent single-carrier STAR receivers to the subcarriers without joint multi-carrier processing or feedback (i.e., no frequency gain). We compute the channel identification error by means of a scalar product, i.e., $\min \|1 \pm \underline{H}_{k,n}^H \widehat{\underline{H}}_{k,n}/M\|^2$. Then, we evaluate the average

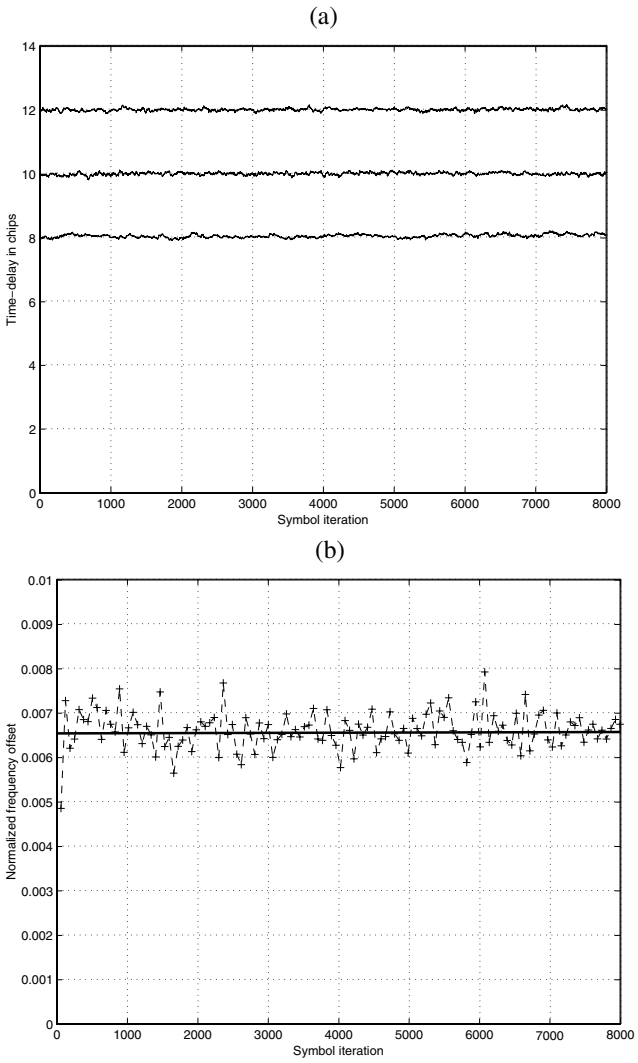

Fig. 2. Acquisition and tracking of (a): time-delays and (b): carrier frequency offset.

channel identification error by averaging over carriers and time. Simulation results show that averaging the parameters common to all subcarriers and combining the channel parameters with high correlation significantly reduce the channel identification error. The improvement in channel identification is as high as 8.5 dB for an operating SNR level of -2.9 dB (see Table III).

D. MT-CDMA, MC-DS-CDMA, and DS-CDMA Performance Comparison

This section is dedicated to the performance comparison of the new MC-STAR configurations: MT-CDMA and MC-DS-CDMA with DBPSK, DQPSK and D8PSK modulations. The link-level curves provide a good picture of the performance of each system. But limiting comparisons to BER performance is not sufficient because the data rate is not equal for all configurations. Hence, we translate the link-level results into system-level results in terms of total throughput (or spectrum efficiency) under the following assumptions: 1) all users are received with equal power on all subcarriers (i.e., perfect per-carrier PC); 2) all the cells have the same load as the target cell C; 3) inter-carrier interference includes signals from all other

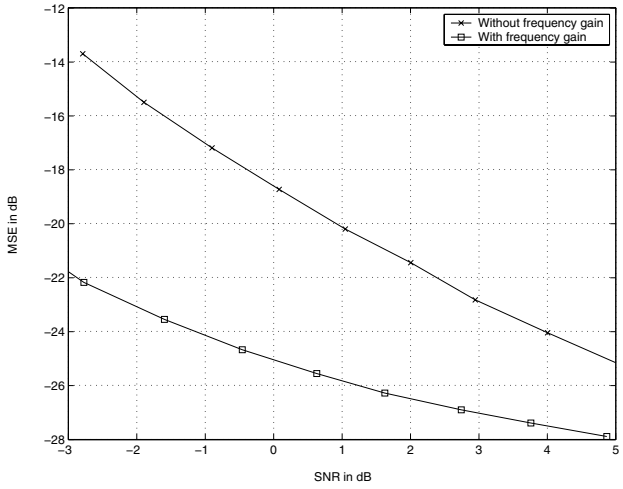

Fig. 3. Channel identification MSE in dB of MC-STAR vs. SNR in dB for $N_c = 5$ with and without frequency gain.

subcarriers for MT-CDMA but only signals from adjacent subcarriers for MC-DS-CDMA (i.e., $N_i = 1$ or 2 for MC-DS-CDMA and $N_i = N_c$ for MT-CDMA); 4) the out-cell to in-cell interference ratio f is set to 0.6. Given the link-level required SNR at the base station $SNR_{req} = L/(N_i[(1+f)C-1])$, the maximum number of users that can access the system can be calculated as $C_{max} = \lfloor \frac{L+N_i SNR_{req}}{(1+f)N_i SNR_{req}} \rfloor$, where $\lfloor . \rfloor$ is the floor function. The total throughput is hence $\mathcal{T}_{max} = C_{max} \times R_b = C_{max} \times R_s \times \log_2(\mathcal{M})$, where R_b and R_s are the bit rate and the symbol rate over all subcarriers, respectively. We also define the spectrum efficiency as $\mathcal{E}_{max} = \mathcal{T}_{max}/BW$.

In Table III, we provide the required SNR and the total throughput of DBPSK, DQPSK and D8PSK modulated data with low mobility (5 kmph) for DS-CDMA, MT-CDMA, and MC-DS-CDMA. Qualitatively, the link-level performance leads to the same conclusions as the throughput performance. This is explained by the close data-rate ranges of the different configurations (refer to Table II).

Table III shows that for DBPSK and DQPSK modulations, when N_c is low, we can improve the system performance by increasing the number of subcarriers. But a gain saturation is encountered as the number of subcarriers increases. Indeed, with a large number of subcarriers the inter-carrier interference becomes dominant and degrades the overall performance of the receiver, and a lower number of subcarriers reduces the frequency gain. We can conclude that for each MC-STAR configuration there exists an optimum value of N_c which results in maximum throughput.

Rapid link-level deterioration is seen with D8PSK, but the deterioration is less dramatic for DS-CDMA and MC-DS-CDMA than for MT-CDMA. Indeed, higher order modulation is more sensitive to the residual frequency offsets after recovery. In a multi-carrier environment the residual-frequency offsets for each subcarrier accumulate in the reconstructed data before detection. This process degrades the orthogonality of subcarriers and makes accurate symbol detection difficult to achieve for high-order modulations especially when the number of subcarriers is large[7]. Single-carrier DS-CDMA, not affected by this phenomenon, has the best performance for D8PSK modulation. This degradation is smaller for MC-DS-CDMA than for MT-CDMA because the subcarrier spacing is higher.

We also observe that MT-CDMA outperforms MC-DS-CDMA with DBPSK and DQPSK modulations when the number of subcarriers is low. Indeed the BER improvement due to using longer spreading sequences and exploiting the subcarrier correlation or frequency gain is higher than the degradation caused by the inter-carrier interference. Moreover, due to the reduced subcarrier bandwidth, MC-DS-CDMA has less frequency diversity, while MT-CDMA is better able to exploit path diversity and achieves better performance. But when the number of subcarriers is high enough the inter-carrier interference becomes dominant especially for high-order modulations (i.e., D8PSK) and MC-DS-CDMA outperforms MT-CDMA because it is more robust to inter-carrier interference.

The throughput results show that D8PSK is the least spectrum-efficient modulation scheme for all MC-STAR configurations. In Table III we fix the modulation scheme and highlight the most spectrum-efficient MC-STAR configuration. For DBPSK and DQPSK, MT-CDMA has the best link-level performance and the highest throughput. MT-CDMA with five subcarriers outperforms all other configurations for DBPSK and DQPSK. It provides a bandwidth efficiency 15 to 30% higher than that achievable with single-carrier CDMA. For D8PSK modulation, the single-carrier DS-CDMA has the best performance.

V. Conclusions

In this contribution we proposed a spectrum-efficient receiver for multi-carrier systems named MC-STAR. It performs blind channel identification and equalization as well as fast and accurate joint synchronization in time and frequency using a simple linear regression approach. MC-STAR supports both the MT-CDMA and MC-DS-CDMA air interfaces. We analyzed its performance in an unknown time-varying Rayleigh channel with multipath, carrier offset and cross-correlation between subcarrier channels. Simulation results confirm the accuracy of the joint time/frequency synchronization. They also confirm that for each MC-STAR configuration there exists an optimum number of subcarriers which results in maximum throughput. A higher number of subcarriers increases the inter-carrier interference, while a lower number of subcarriers reduces the frequency gain. With four receiving antennas and five MT-CDMA subcarriers in 5 MHz bandwidth, MC-STAR provides about 1.2 bps/Hz at low mobility for DBPSK. This bandwidth efficiency is 30% higher than that achievable with single-carrier CDMA for DBPSK.

References

[1] L. Hanzo, T. Keller, M.S. Munster, and B.J. Choi, *OFDM and MC-CDMA for Broadband Multiuser Communications, WLANs and Broadcasting*, John Wiley & Sons Inc, 2003.

[7] In an ongoing study, we are investigating the incorporation of inter-carrier-interference suppression to allow a more efficient MC-STAR implementation with high-order modulations.

TABLE II

PARAMETERS OF EACH MULTI-CARRIER SYSTEM CONFIGURATION.

Parameter	DS-CDMA	MT-CDMA				MC-DS-CDMA				Comment
λ	-	1				L				subcarrier spacing parameter
N_c	1	3	5	7	9	3	5	7	9	number of subcarriers
L	64	128	256	384	512	64	64	64	64	spreading factor
R_c in Mcps	3.840	3.840				1.920	1.280	0.960	0.768	chip rate
P	3	3				2	1	1	1	number of paths per subcarrier
K_f	0	1	2	3	4	0				averaging window span in subcarriers
R_s in kbaud	60	90	75	70	67.5	90	100	105	108	symbol rate over all subcarriers
R_b for DBPSK in kbps	60	90	75	70	67.5	90	100	105	108	peak rate for DBPSK
R_b for DQPSK in kbps	120	180	150	140	135	180	200	210	216	peak rate for DQPSK
R_b for D8PSK in kbps	180	270	225	210	202.5	270	300	315	324	peak rate for D8PSK
BW_{nor}	1	1.016				1				bandwidth normalized vs. DS-CDMA

TABLE III

REQUIRED SNR, CAPACITY, MAXIMUM THROUGHPUT, AND SPECTRAL-EFFICIENCY OF DS-CDMA, MT-CDMA, AND MC-DS-CDMA WITH JOINT TIME AND FREQUENCY SYNCHRONIZATION FOR DBPSK, DQPSK, AND D8PSK (BEST PERFORMANCE VALUES FOR EACH MODULATION ARE IN BOLD).

MC-STAR configuration	DS-CDMA	MT-CDMA				MC-DS-CDMA			
N_c	1	3	5	7	9	3	5	7	9
Modulation	DBPSK								
SNR_{req} in dB	-1.8	-2.4	**-2.9**	-2.45	-1.7	-0.94	-1.2	-1.3	-0.96
C_{max}	61	46	**63**	60	53	30	29	29	27
$\mathcal{T}_{max}$ in kbps	3660	4140	**4725**	4200	3577.5	2700	2900	3045	2916
$\mathcal{E}_{max}$ in bps/Hz	0.95	1.08	**1.23**	1.09	0.93	0.70	0.75	0.79	0.76
Modulation	DQPSK								
SNR_{req} in dB	1.0	0.7	**0.4**	1.4	3.0	1.9	1.9	2.0	2.0
C_{max}	32	23	**29**	25	18	15	15	14	13
$\mathcal{T}_{max}$ in kbps	3840	4140	**4350**	3500	2430	2700	3000	2940	2808
$\mathcal{E}_{max}$ in bps/Hz	1.00	1.08	**1.13**	0.91	0.63	0.70	0.78	0.77	0.73
Modulation	D8PSK								
SNR_{req} in dB	**5.4**	5.8	6.7	9.0	12.4	6.2	6.5	6.8	7.2
C_{max}	**12**	7	7	4	2	6	5	5	4
$\mathcal{T}_{max}$ in kbps	**2160**	1890	1575	840	405	1620	1500	1575	1296
$\mathcal{E}_{max}$ in bps/Hz	**0.56**	0.49	0.41	0.22	0.10	0.42	0.39	0.41	0.34

[2] H. Steendam and M. Moeneclaey, "The effect of carrier frequency offsets on downlink and uplink MC-DS-CDMA", *IEEE J. Select. Areas in Commun.*, vol. 19, no. 12, pp. 2528-2536, December 2001.

[3] W. Nabhane and H.V. Poor, "Blind joint equalization and multiuser detection in dispersive MC-CDMA/MC-DS-CDMA/MT-CDMA channels", *MILCOM 2002*, vol. 2, pp. 814-819.

[4] Q. Tian and K. Ben Letaief, "ML estimation and correction of frequency offset for MC-CDMA systems over fading channels", *IEEE VTC 2001 Spring*, vol. 1, pp. 571-575.

[5] A. Feng, Q. Yin, Z. Zhao, and H. Zhang, "Blind space-time equalization/decoding with carrier frequency synchronization in multicarrier CDMA systems", *IEEE International Symposium on Circuits and Systems 2002*, vol. 2 , pp. 500-503.

[6] A. Feng, Q. Yin, and K. Deng, "Blind channel estimation in synchronous MC-CDMA system with consideration of carrier offset compensation", *IEEE VTC 2002 Spring*, vol. 2, pp. 660-664.

[7] J.-H. Deng and T.-S. Lee, "An Iterative maximum SINR receiver for multicarrier CDMA systems over a multipath fading channel with frequency offset", *IEEE Trans. on Wireless Commun.*, vol. 2, no. 3, pp. 560-569, May 2003.

[8] D. Darsena and F. Verde, "Time-frequency synchronisation algorithm for MC-CDMA systems in LMDS applications", *Electronics Letters*, vol. 39, no. 10, pp. 806-807, May 2003.

[9] B. Smida, S. Affes, J. Li, and P. Mermelstein, "A spectrum-efficient multicarrier CDMA array-receiver with time/frequency synchronization", submitted to *IEEE Trans. on Wireless Commun.*, in review.

[10] S. Affes and P. Mermelstein, "A new receiver structure for asynchronous CDMA: STAR the spatio-temporal array-receiver", *IEEE J. Select. Areas in Commun.*, vol. 16, no. 8, pp. 1411-1422, October 1998.

[11] L. Yang and L. Hanzo, "Performance of generalized multicarrier DS-CDMA over Nakagami-m fading channels", *IEEE Trans. on Commun.*, vol. 50, no. 6, pp. 956-966, June 2002.

[12] S. Kondo and L. Milstein, "Performance of multicarrier DS CDMA Systems", *IEEE Trans. on Commun.*, vol. 44, no. 2, February 1996.

[13] Q.M. Rahman and A.B. Sesay, "Performance analysis of MT-CDMA system with diversity combining", *IEEE MILCOM 2001*, vol. 2 , pp. 1360-1364.

[14] S. Affes and P. Mermelstein, "Adaptive space-time processing for wireless CDMA", *Book Chapter, Adaptive Signal Processing: Application to Real-World Problems,* J. Benesty and A.H. Huang, Eds., Springer, Berlin, January 2003.

[15] W.C. Jakes, et al, *Microwave Mobile communications*, New York: Wiley, 1974.

[16] B. Natarajan, C.R. Nassar, and V. Chandrasekhar, "Generation of correlated Rayleigh fading envelopes for spread spectrum applications", *IEEE Communications Letters*, vol. 4, no.1 , pp. 9-11, January 2000.

[17] J. Li, *Multitone-CDMA Array Receiver for Increased Spectrum Efficiency over Broadband Channels*, MSc dissertation, INRS-EMT, Ref. 806, 2003.

[18] K. Cheikhrouhou, S. Affes, and P. Mermelstein, "Impact of synchronization on performance of enhanced array-receivers in wideband CDMA networks", *IEEE J. Select. Areas in Commun.*, vol. 19, no 12, pp. 2462-2476, December 2001.